

Supplementary information

Superior sulfur infiltration into carbon mesosponge via chemical reaction for enhanced cycling stability in lithium-sulfur batteries

Tianshu Liu ^a, Koki Fujita ^a, Ayako Kawase ^{b,*}, Zheng-Ze Pan ^c, Takuma Kuroda ^d, Shinichiroh Iwamura ^{c,d}, and Hiroto Nishihara ^{a,c*}

^a Institute of Multidisciplinary Research for Advanced Materials, Tohoku University, 2-1-1 Katahira, Aoba-ku, Sendai, Miyagi, 980-8577, Japan

^b ENAX Inc., Tokyo, 112-0003, Japan

^c Advanced Institute for Materials Research (WPI-AIMR), Tohoku University, 2-1-1 Katahira, Aoba-ku, Sendai, Miyagi, 980-8577, Japan

^d 3DC Inc., Sendai, Miyagi, 980-8577, Japan

* Corresponding author.

E-mail addresses: akawase@24-m.com (Ayako Kawase);

hirotomo.nishihara.b1@tohoku.ac.jp (H. Nishihara).

Experimental section

CMS synthesis

The synthesis of CMS was following the process reported in previous research.¹ Commercially procured magnesium oxide (brand name: MF150, Kyowa Chemical Industry) was used as the CVD template for the CMS synthesis. 15.5 g of MF150 was weighed and placed into a quartz reactor. The reactor was then positioned in the Rotary Kiln CVD apparatus and vacuumized prior to the CVD program. The temperature of the reactor was raised to 900 °C under the protection of Ar gas (400 mL min⁻¹). After a holding time of 30 minutes, 20% of CH₄ (80 mL min⁻¹) was introduced into the reactor and maintained for 90 minutes at 900 °C, and the Ar flow rate was adjusted to (320 mL min⁻¹). Following the cessation of CH₄, the reactor was kept at 900 °C under Ar gas (400 mL min⁻¹) for an additional 30 minutes. Once the reactor had cooled down to room temperature, it was removed from the apparatus. It was observed that the powder inside the reactor exhibited a black color at the gas inlet side and a grey color at the gas outlet side, indicating nonhomogeneous carbon deposition on the template. To achieve a more uniform CMS, the reactor was repositioned in the Rotary Kiln with the opposite direction, and a 90-minute CVD program with the same temperature and gas flow was performed again, resulting in additional carbon deposition on the initially grey-colored sample. Following these two CVD cycles, both the gas inlet and outlet sides of the sample exhibited black powder. Next, 10 g of obtained carbon coated MgO was immersed into 200 mL of 5 mol L⁻¹ HCl (Fujifilm Wako Pure Chemicals). The mixture was stirred overnight to fully remove the MgO template. The sample was then washed six times with pure water to eliminate any excess HCl. The resulting CMS was partially immersed in pure water to prepare the cS(79)/wCMS directly. The remaining portion of CMS was made into a dried powder through two rounds of acetone replacement and 6 hours of vacuum drying at 150 °C. This dried powder would be used for preparing mS(79)/CMS.

Preparation of sulfur/carbon composites

To prepare cS(79)/wCMS, 2.996 g of sodium sulfide nonahydrate (Na₂S·9H₂O, Kishida Chemical) was dissolved in 40 mL of pure water to create a Na₂S solution. Next, 1.200 g of elemental sulfur (Kanada Pharmaceutical Industries) was dissolved in the Na₂S solution. The mixture was stirred at 70 °C for 2 hours, forming a sodium polysulfide solution with a stoichiometric composition of Na₂S₄, which turned from colorless to dark orange as the sulfur fully dissolved. This sodium polysulfide solution was then added to a 200 mL wCMS dispersion (approximately 256 mg of wCMS) and stirred at 70 °C for

over 16 hours. Subsequently, 100 mL of 2 mol/L formic acid (Kishida Chemical) was slowly added, and the mixture was stirred for another 2 hours at 70 °C to deposit sulfur into the wCMS. After the reaction, the mixture was filtered, and the composite was washed with pure water. The sulfur/wCMS powder was vacuum dried at 60 °C for over 12 hours. A mild heat treatment at 250 °C for 30 minutes under an argon atmosphere was applied to remove residual sulfur on the wCMS surface.

To prepare mS(79)/CMS, 1.200 g of elemental sulfur was physically mixed with 0.300 g of CMS powder using a mortar. After thorough grinding, the mixture was heated at 155 °C for 12 hours under an argon atmosphere with a flow rate of 100 mL min⁻¹. Following this, the mixture underwent an additional heat treatment at 250 °C for 30 minutes to remove excess sulfur from the surface of the CMS particles. The same process was applied to prepare the corresponding sulfur/carbon composites by using AC (MSC30, Kansai Coke and Chemicals Co.) and GO (Graphenea, Inc.) as carbon scaffolds, forming cS(79)/AC, mS(79)/AC, as well as cS(86)/GO, and mS(86)/GO.

Material characterizations

The microscopic morphology of the samples was observed using a scanning electron microscope (SEM; S-4800, Hitachi). Elemental mapping was performed with a SEM (JSM-7800F, JEOL) equipped with an energy dispersive X-ray spectrometer (Oxford Instruments). X-ray photoelectron spectroscopy (XPS; ESCA-3400, Shimadzu) with Al K α radiation was applied to analyze the lithium anode surface. The crystallinity of the samples was examined by using an X-ray diffractometer (MiniFlex600, Rigaku) with Cu K α radiation at 40 kV and 15 mA. The pore structure of samples was analyzed by using Belsorp-mini II (MicrotracBEL Corp.) at -196 °C. The specific surface area (S_{BET}) was calculated using the Brunauer-Emmett-Teller (BET) method. The total pore volume (V_{total}) was determined from the N₂ adsorption amount at P/P₀=0.96. The pore-size distribution was determined using the Barrett–Joyner–Halenda (BJH) method based on the adsorption isotherm. Water vapor adsorption/desorption isotherms were measured by using Belsorp-max (MicrotracBEL Corp.). Sulfur loading content in the composite determined through thermogravimetric analysis (TGA; TGA-50, Shimadzu) under a nitrogen atmosphere. Raman spectra were measured using a spectrometer (LabRAM HR-800, HORIBA) with a 532 nm laser. The number of carbon edge sites was analyzed by using an in-house vacuum temperature programmed desorption (TPD) system, which measured the total gas evolution as the sample was heated to 1800 °C. The UV-vis spectra of the Na₂S₄ solution before and after adding CMS or GMS were recorded using a UV-vis spectrophotometer (V-670, Jasco).

Cathode preparation

The obtained S/CMS composite was ground for 10 minutes in a mortar. Multi-wall Carbon Nanotubes (CNTs, Cheap Tubes Inc) were then added to the mortar and grinding continued for another 10 minutes. The mixed powder was weighed and transferred into a plastic bottle. Subsequently, a binder of polyacrylic acid (PAA, Sigma Aldrich) was added, with a controlled weight content ratio of sulfur: CMS+CNT: PAA at 60:38:2. To prepare the electrode slurry, water was added to the composite in a weight ratio of 21:79. To achieve a homogeneous slurry, the mixture was placed in a vial for 5 hours magnetic stirring. The prepared slurry was then uniformly spread onto a carbon-coated aluminum sheet (EQ-CC-Al-18u, MTI) at a controlled coating speed of 5 mm s^{-1} . The solvent was evaporated using an $80 \text{ }^{\circ}\text{C}$ hot plate. Circular sheets with a diameter of 12 mm were punched out from the coated sheet to create the electrodes. These electrodes were vacuum dried at $60 \text{ }^{\circ}\text{C}$ for more than 12 hours. The pouch cell cathode with a 12 cm^2 rectangular shape was prepared using the same process. The areal sulfur loading of the electrodes ranged from 2.7 to 3.3 mg cm^{-2} .

Electrochemical measurement

The CR2032 coin cell was assembled with a Celgard 2400 separator positioned between the S/CMS cathode and a lithium metal sheet anode (Honjo Metal Co., Ltd.). The electrolyte consisted of 1 mol L^{-1} lithium bis (trifluoro methanesulfonyl) imide (Sigma Aldrich), 1 mol L^{-1} LiNO_3 (Sigma Aldrich) and 0.08 mol L^{-1} $\text{La}(\text{NO}_3)_3$ (Sigma Aldrich) dissolved in a mixture of 1, 2-dimethoxyethane and 1, 3-dioxolane in a 1:1 volume ratio. A total volume of $70 \text{ }\mu\text{L}$ electrolyte was used for evaluating the coin cell electrochemical performance. The pouch cell was prepared using the same electrolyte with a total volume of $227 \text{ }\mu\text{L}$. Galvanostatic discharge/charge tests were conducted using LAND battery testing system. The applied potential range was limited to 1.8 V to 2.45 V . Electrochemical impedance spectrum (EIS) measurements were conducted using a Bio-Logic VMP3 instrument, with a frequency range of 10 mHz to 1 MHz at a perturbation amplitude of 10 mV .

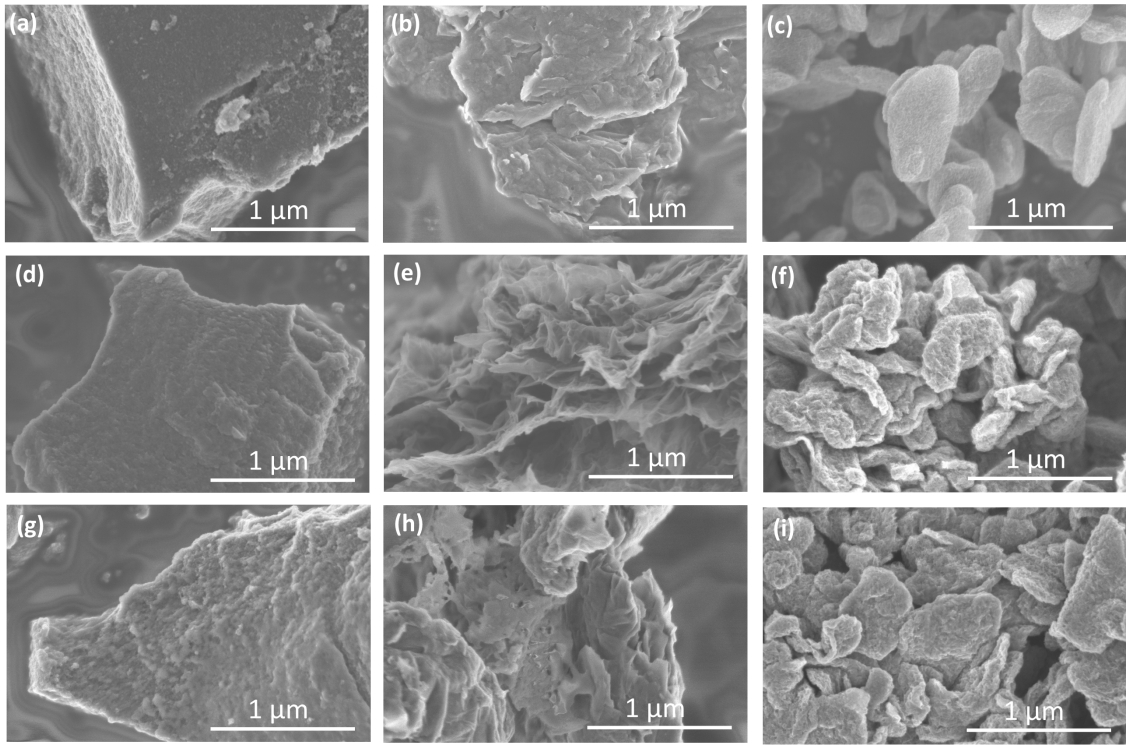


Figure S1. SEM images of (a) AC, (b) GO, (c) CMS, (d) cS/AC, (e) cS/GO, (f) cS/CMS, (g) mS/AC, (h) mS/GO, and (i) mS/wCMS.

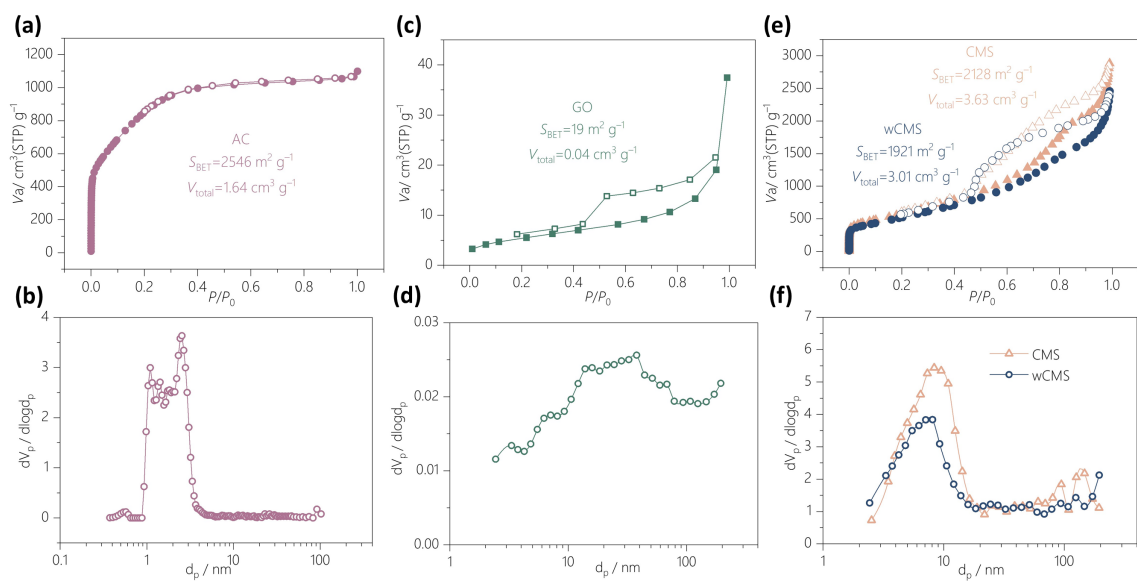


Figure S2. Texture properties of pure carbons. (a,c,e) N₂ adsorption-desorption isotherms of (a) AC, (c) GO, and (e) CMS. (b,d,f) Pore-size distributions of (b) AC, (d) GO, and (f) CMS.

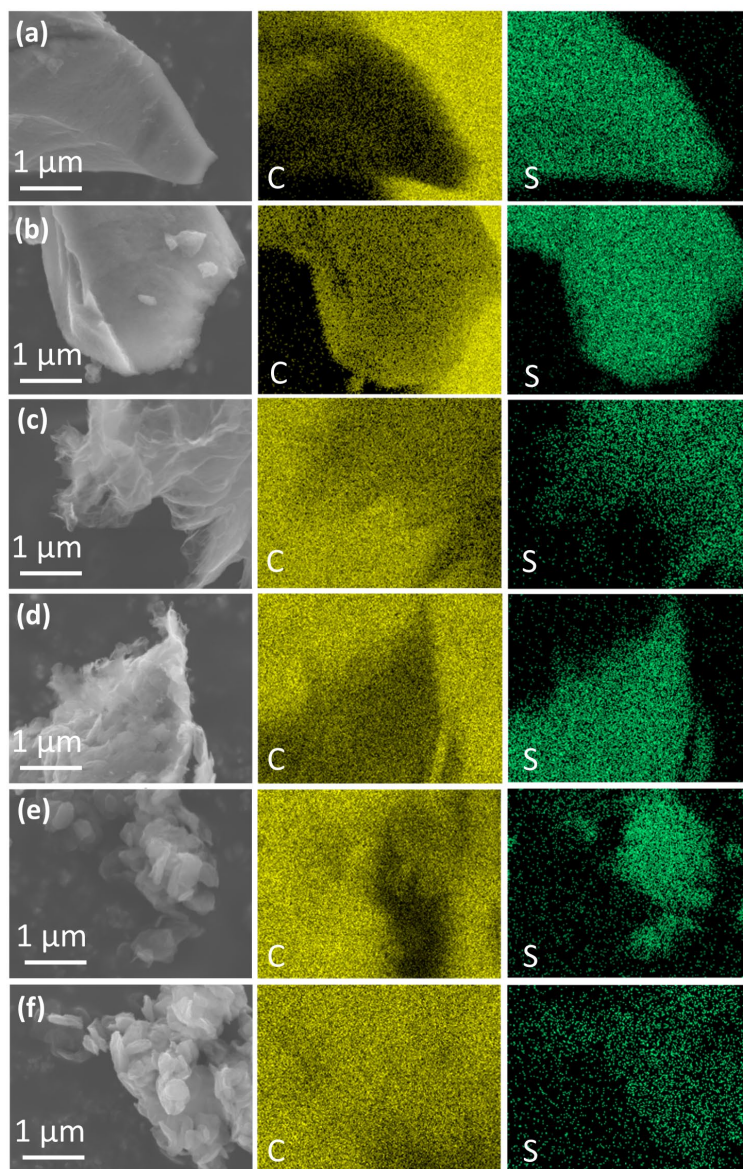


Figure S3. Elemental mapping of sulfur/carbon composite. (a) cS(79)/AC, (b) mS(79)/AC, (c) cS(86)/GO, (d) mS(86)/GO, (e) cS(79)/wCMS, and (f) mS(79)/CMS. The yellow color for carbon signals strongly appears at background due to the use of carbon tapes for the fixation of samples.

Table S1. Texture properties of carbons and its maximum sulfur content.

Carbon scaffold	S_{BET} ($\text{m}^2 \text{g}^{-1}$)	V_{total} ($\text{cm}^3 \text{g}^{-1}$)	Maximum sulfur content (wt%)	Maximum sulfur content (g-S/g-carbon)
AC	2546	1.64	77	3.39
GO	19	0.04	7	0.08
CMS	2128	3.63	88	7.51
wCMS	1921	3.01	86	6.23

* The maximum sulfur content is calculated under the assumption that the carbon pores are completely filled with sulfur.

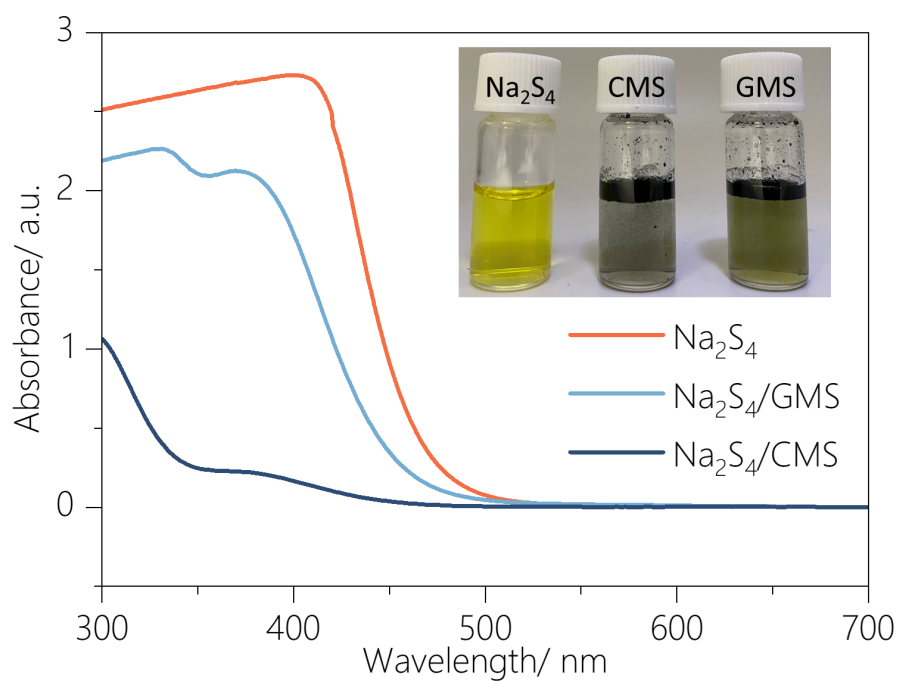


Figure S4. UV-vis spectra of the aqueous Na_2S_4 solution before and after adding CMS or GMS (inset: image of pure Na_2S_4 solution and Na_2S_4 solutions after adding CMS or GMS for 30 minutes).

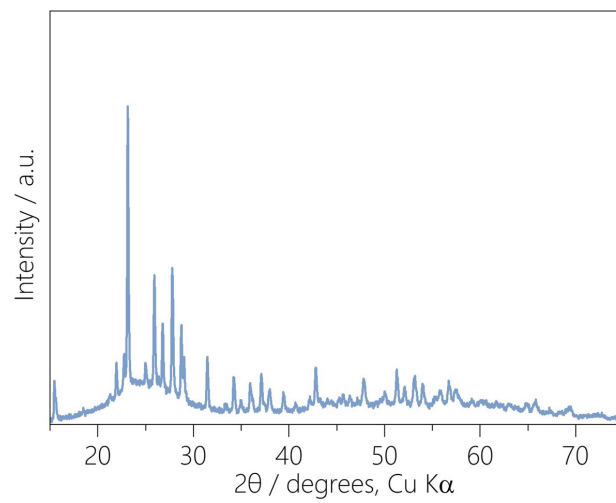


Figure S5. XRD pattern of pS(79)/CMS.

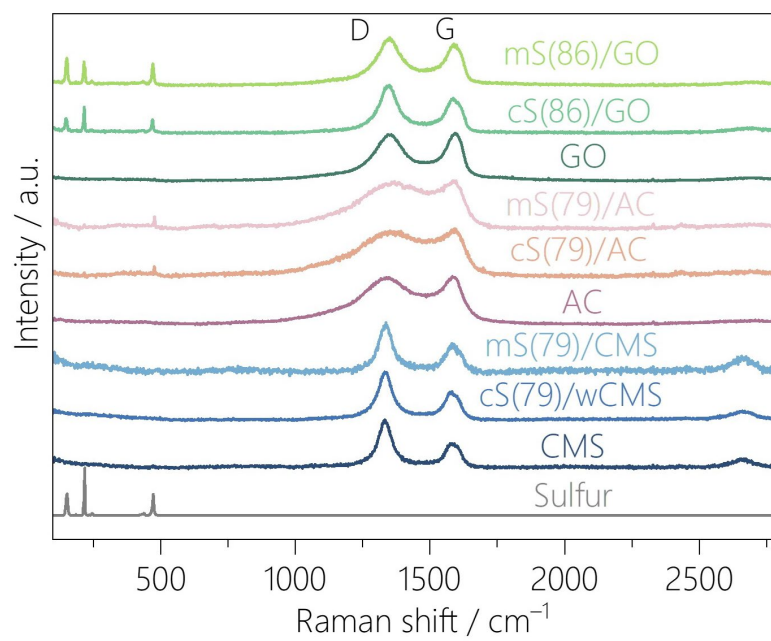


Figure S6. Raman spectra of carbon scaffolds and sulfur/carbon composites.

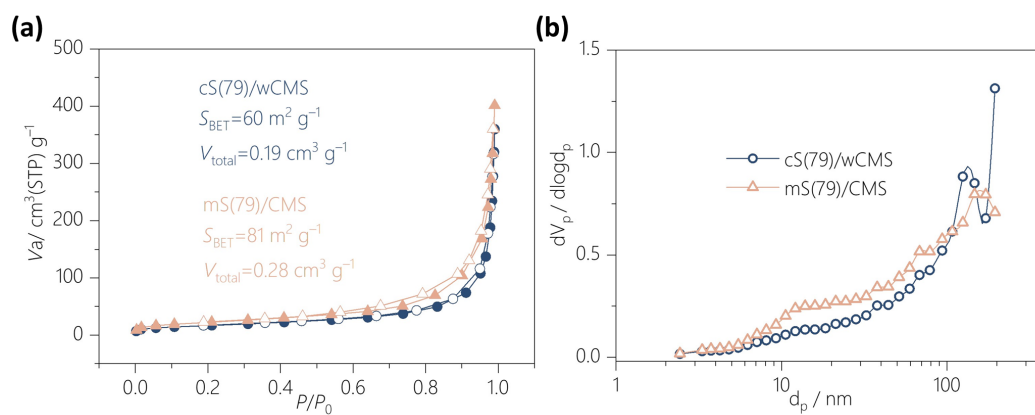


Figure S7. (a) N_2 adsorption-desorption isotherms of mS(79)/CMS and cS(79)/wCMS. (b) Pore-size distributions.

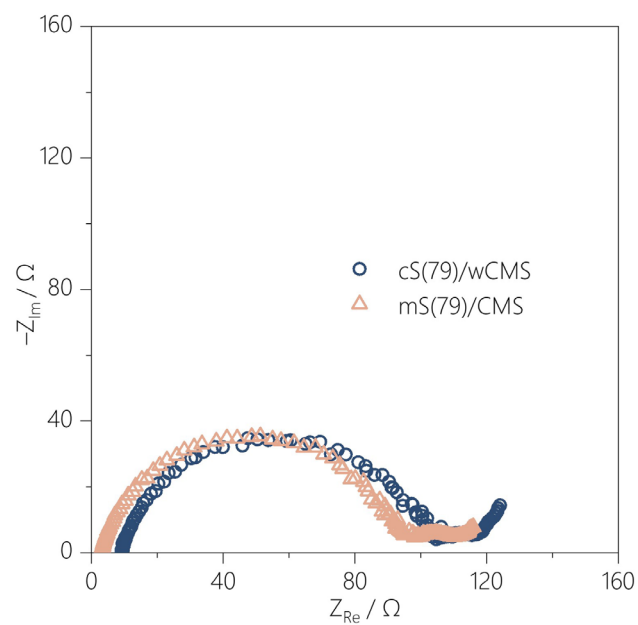


Figure S8. Nyquist plots at open circuit potential before GCD measurement.

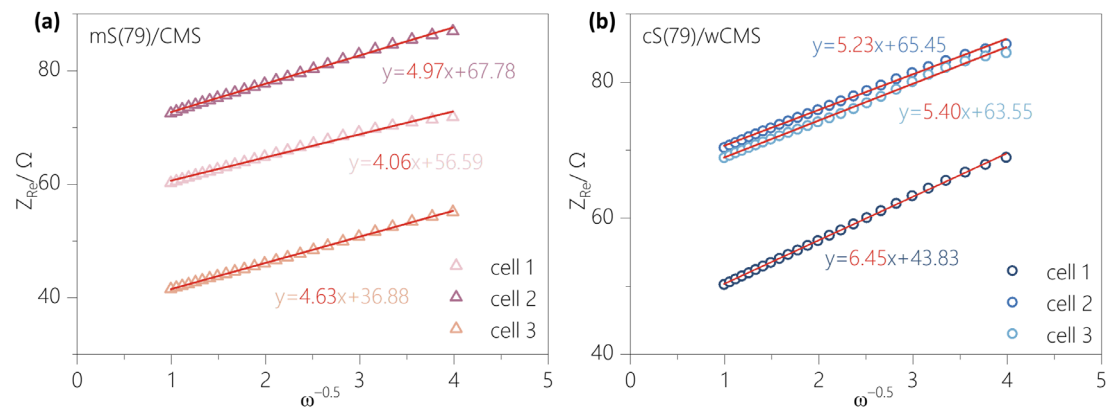


Figure S9. The relationship between real part of impedance and the inverse square root of angular frequency across multiple cells. (a) mS(79)/CMS. (b) cS(79)/wCMS.

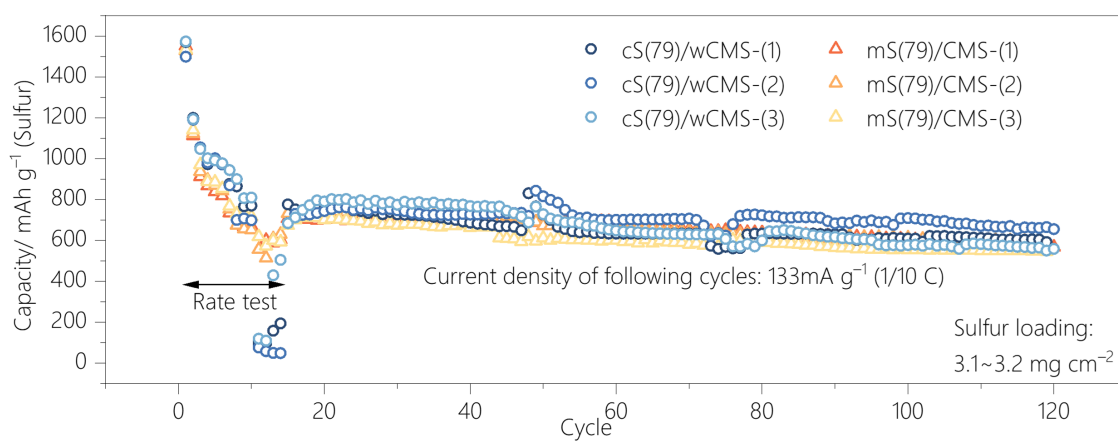


Figure S10. Cycling stability results of S/CMS composites across multiple cells.

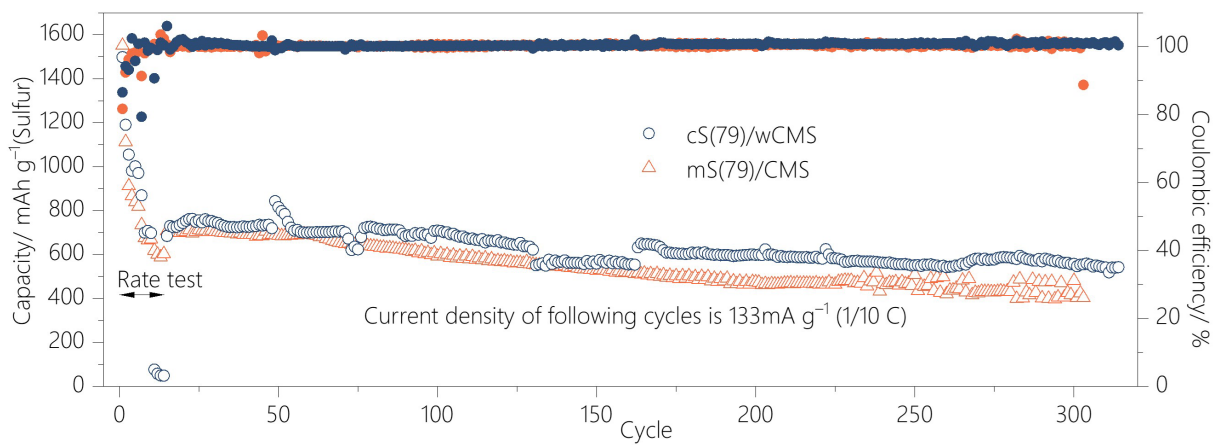


Figure S11. Long-term cycling stability of S/CMS composites.

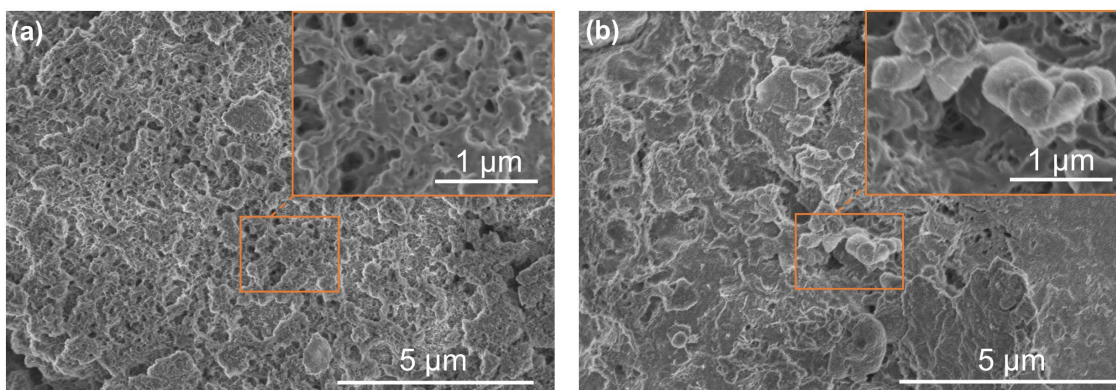


Figure S12. Electrode morphology of different S/CMS composites after 100 cycles. (a) SEM image of mS(79)/CMS. (b) SEM image of cS(79)/wCMS.

Table S2. Theoretical calculations of CMS pore volume and Sulfur volume expansion.

Sample	$V_{\text{total of CMS}}$ ($\text{cm}^3 \text{g}^{-1}$)	$V_{\text{sulfur}}/ V_{\text{total of CMS}}$	$V_{\text{lithium sulfide}}/ V_{\text{total of CMS}}$
mS(79)/CMS	3.63	50%	89%
cS(79)/wCMS	3.01	60%	108%
mS(73)/CMS	3.63	36%	64%
cS(73)/wCMS	3.01	43%	78%

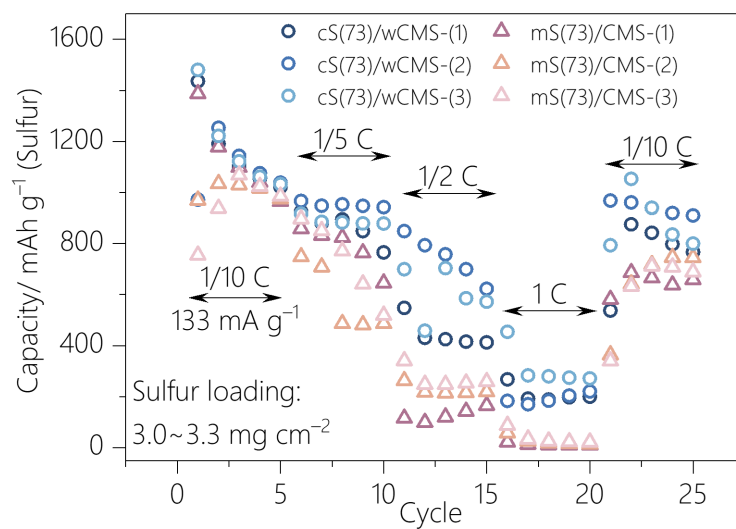


Figure S13. Rate performance tests of S/CMS composites with an optimized sulfur content (73 wt%) across multiple cells.

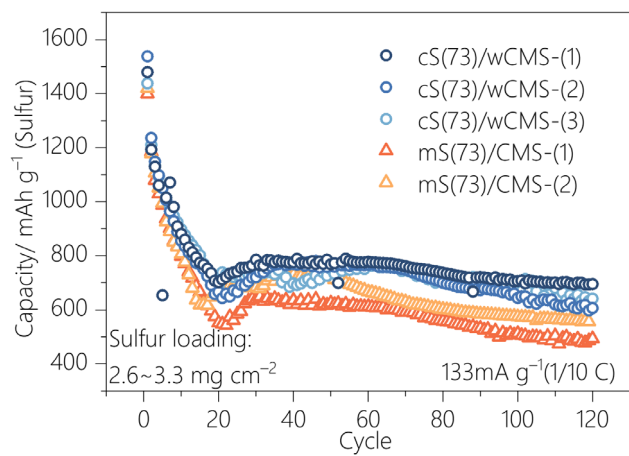


Figure S14. Cycling stability tests of S/CMS composites with an optimized sulfur content (73 wt%) across multiple cells.

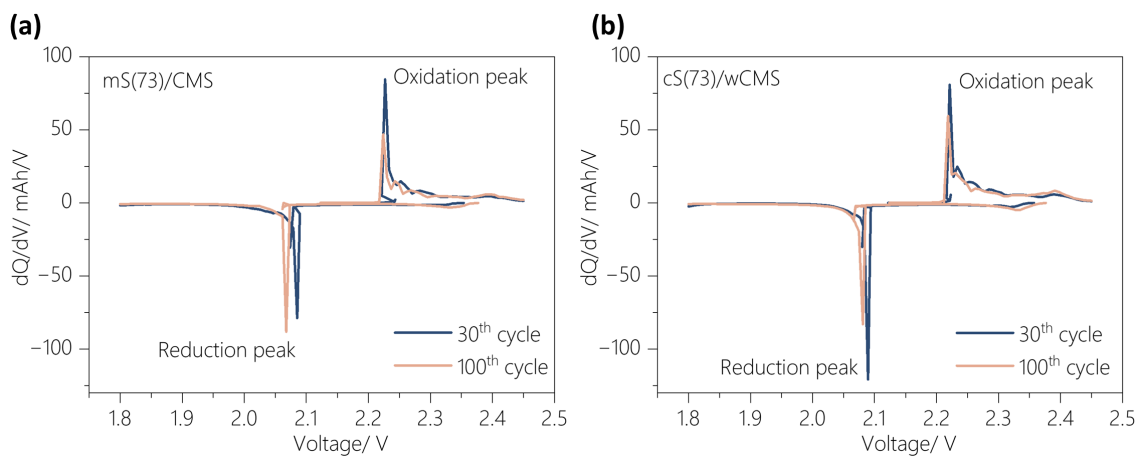


Figure S15. dQ/dV curves derived from GCD measurements. (a) mS(73)/CMS. (b) cS(73)/wCMS.

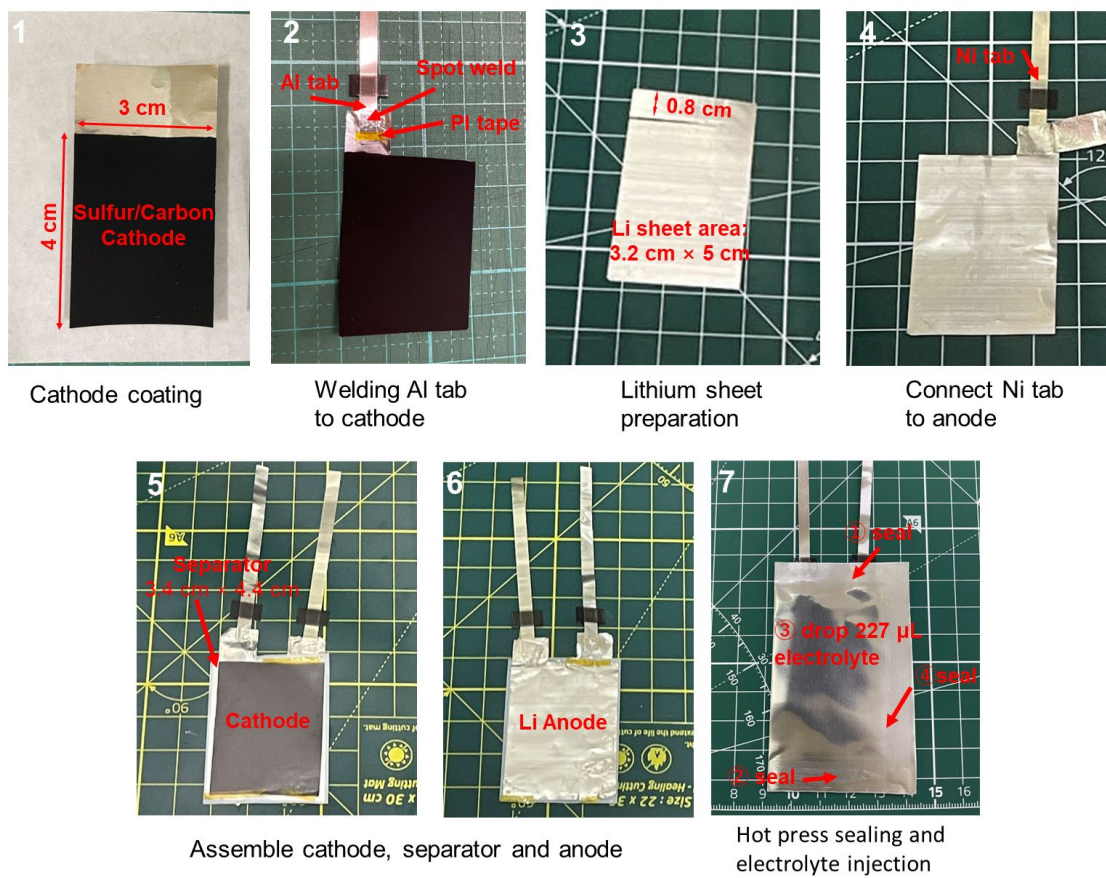


Figure S16. Cycling test of a pouch cell using cS(73)/wCMS.

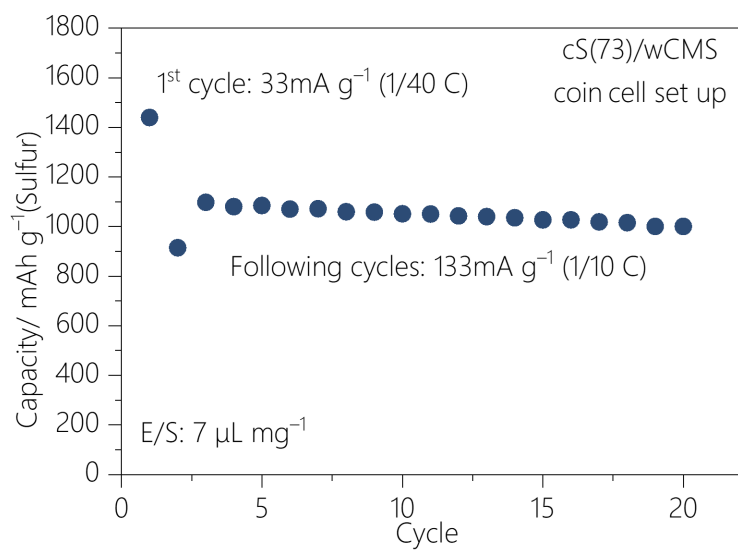


Figure S17. Cycling test of a coin cell with low E/S ratio.

Table S3. Comparison of capacity retention and energy density of cS(73)/wCMS with some representative lithium sulfur pouch cell.

Sulfur scaffold	Electrolyte	Sulfur content (wt%)	Sulfur loading (mg cm^{-2})	E/S ($\mu\text{L/mg}$)	Current density	Capacity retention (mAh g^{-1})	Rate capability in coin cell (mAh g^{-1})	Ref.
wCMS	1.0 M LiTFSI+1.0 M LiNO ₃ +0.08 M La(NO ₃) ₃ in DOL/DME	73	2.7	7	1/10 C	1192 (After 30 cycles)	268 (1 C)	This work
Graphitic carbon nitride	1.0 M LiTFSI+0.4 M LiNO ₃ in DOL/DME	70	9	3.2	1/10 C	947 (After 48 cycles)	169 (4 C)	2
CNT	1.0 M LiTFSI+2.0 wt.% LiNO ₃ in DOL/DME/HME	60	7.6	3	1/40 C	748 (After 27 cycles)	869 (0.3 C)	3
Nitrogen-doped carbon	1.0 M LiTFSI+0.2 M LiNO ₃ in DOL/DME	80	1.2	10	1/5 C	1031 (After 100 cycles)	563 (1 C)	4
ZnS/rGO	1.0 M LiTFSI+1.0 wt.% LiNO ₃ in DOL/DME	70	2	–	–	261 (After 50 cycles)	945 (1 C)	5
MWCNT	0.3 M LiTFSI+0.25 M LiNO ₃ in DME/MTBE	70	16	1.3	0.3 mA cm^{-2}	376 (After 75 cycles)	–	6
Ketjen Black	2.0 M LiTFSI+1.0 wt.% B(C ₆ F ₅) ₃ in DOL	60	3.5	3	1/10 C	1000 (After 20 cycles)	778 (0.2 C)	7
Core-shell hollow sphere	1.0 M LiTFSI+0.1 M LiNO ₃ in DOL/HFE	70	3.33	10	0.2 A g^{-1}	1103 (After 30 cycles)	509 (4 C)	8

VS4@rGO	1.0 M LiTFSI+0.2 M LiNO ₃ in DOL/DME	66	5	7	1/7 C	730 (After 50 cycles)	410 (4 C)	9
Nitrogen-doped carbon	1.0 M LiTFSI+0.5 M LiNO ₃ in DOL/DME	60	2.4	5	1/10 C	930 (After 100 cycles)	–	10
MWCNT	0.5 M LiTFSI+0.4 M LiNO ₃ in DOL/DME	90	3.1	9.5	1/2 C	838 (After 80 cycles)	550 (5 C)	11
Ketjen Black with MoB	1.0 M LiTFSI+0.2 M LiNO ₃ in DOL/DME	85	3.5	4.5	1/20 C	947 (After 55 cycles)	600 (1 C)	12
CoPc@carbon nanofibre	1.0 M LiTFSI+2.0 wt.% LiNO ₃ in DOL/DME	80	5	4.5	1/2 C	763 (After 200 cycles)	1007 (1 C)	13
CNT+graphene	1.0 M LiTFSI+0.1 M LiNO ₃ in DOL/DME	70	5	3	1/10 C	779 (After 35 cycles)	998 (1 C)	14
CNT	1.0 M LiTFSI in DIPS/DOL/DME	80	6.1	2.7	1/10 C	750 (After 50 cycles)	800 (0.5 C)	15
Three-dimensional Zn, Co, and N codoped carbon nanoframes	1.0 M LiTFSI+2.0 wt.% LiNO ₃ in DOL/DME	68	10	4	1/10 C	900 (After 50 cycles)	894 (2 C)	16
2D ZIF-7	1.0 M LiTFSI+2.0 wt.% LiNO ₃ in DOL/DME	75	2.3	–	1/10 C	901 (After 100 cycles)	511 (5 C)	17

γ -CDMOF on graphene foam	1.0 M LiTFSI+1.0 wt.% LiNO ₃ in DOL/DME	62	7	5	1/10 C	913 (After 100 cycles)	590 (5 C)	18
MOF-TOC	1.0 M LiTFSI+1.0 wt.% LiNO ₃ in DOL/DME	80	7	15	1/10 C	1020 (After 100 cycles)	740 (3 C)	19
Polymer coated MOF	1.0 M LiTFSI+0.2 M LiNO ₃ in DOL/DME	78	3	4.8	1/10 C	726 (After 40 cycles)	567 (5 C)	20
Dual-active-center MOFs	1.0 M LiTFSI+2.0 wt.% LiNO ₃ in DOL/DME	75	3.6	–	1/10 C	850 (After 50 cycles)	716 (5 C)	21
3D COF	1.0 M LiTFSI+2.0 wt.% LiNO ₃ in DOL/DME	80	4.2	4	1/10 C	1031 (After 40 cycles)	729 (3 C)	22
TpBD-Me ₂ COF	1.0 M LiTFSI+0.1 M LiNO ₃ in DOL/DME	75	1.2	–	1/10 C	860 (After 50 cycles)	543 (3 C)	23
COF-coated MOF	1.0 M LiTFSI+0.1 M LiNO ₃ in DOL/DME	75	–	–	1/10 C	752 (After 50 cycles)	701 (3 C)	24

Supporting Calculation 1

Gravimetric energy density (E_g) for pouch cell (Wh kg^{-1}):

$$E_g = \frac{1000 \times C \times V}{m_{Ca} + m_{Li} + m_{Se} + m_{El} + m_{Al}}$$

C : Discharge capacity (mAh).

V : Average output voltage (V). 2.1 V in this case.

m_{Ca} : Mass of cathode, including sulfur, CMS, CNT and binder (mg).

m_{Li} : Mass of lithium anode (mg).

m_{Se} : Mass of separator (mg).

m_{El} : Mass of electrolyte (mg).

m_{Al} : Mass of aluminum current collector (mg).

Reference

1. Liu T, Kaku R, Pan ZZ, Ohwada M, Pirabul K, Li B, et al. Mesoporous nanoplates consisting of seamless graphene frameworks. *Electrochim Acta*. 2024 Apr 20;484.
2. Sun W, Xu L, Song Z, Lin H, Jin Z, Wang W, et al. Coordination Engineering Based on Graphitic Carbon Nitrides for Long-Life and High-Capacity Lithium-Sulfur Batteries. *Adv Funct Mater*. 2024 Apr 3;34(14).
3. Su LL, Yao N, Li Z, Bi CX, Chen ZX, Chen X, et al. Improving Rate Performance of Encapsulating Lithium-Polysulfide Electrolytes for Practical Lithium–Sulfur Batteries. *Angewandte Chemie - International Edition*. 2024 Mar 4;63(10).
4. Qiu D, Zhang X, Zheng D, Ji W, Ding T, Qu H, et al. High-Performance Li-S Batteries with a Minimum Shuttle Effect: Disproportionation of Dissolved Polysulfide to Elemental Sulfur Catalyzed by a Bifunctional Carbon Host. *ACS Appl Mater Interfaces*. 2023 Aug 2;15(30):36250–61.
5. Peng H, Zhang Y, Chen Y, Zhang J, Jiang H, Chen X, et al. Reducing polarization of lithium-sulfur batteries via ZnS/reduced graphene oxide accelerated lithium polysulfide conversion. *Mater Today Energy*. 2020 Dec 1;18.
6. Li H, Feng J, Liu T, Qin K, Zhu X, Suo L. Suppressing sulfur crosstalk lowers the bar of lithium metal anode for practical Li-S pouch cells. *Energy Storage Mater*. 2024 Aug 1;71.
7. Shi T, Liao Y, Kong J, Ji H, Hou T, Huang Z, et al. Quasi-solid-state sulfur cathode with ultralean electrolyte via in situ polymerization. *Energy Storage Mater*. 2024 Sep 1;72.
8. Zhao C, Xu GL, Zhao T, Amine K. Beyond the Polysulfide Shuttle and Lithium Dendrite Formation: Addressing the Sluggish Sulfur Redox Kinetics for Practical High-Energy Li-S Batteries. *Angewandte Chemie - International Edition*. 2020 Sep 28;59(40):17634–40.
9. Luo L, Li J, Yaghoobnejad Asl H, Manthiram A. In-Situ Assembled VS₄ as a Polysulfide Mediator for High-Loading Lithium-Sulfur Batteries. *ACS Energy Lett*. 2020 Apr 10;5(4):1177–85.
10. Kensy C, Härtel P, Maschita J, Dörfler S, Schumm B, Abendroth T, et al. Scalable production of nitrogen-doped carbons for multilayer lithium-sulfur battery cells. *Carbon N Y*. 2020 May 1;161:190–7.
11. Hwang JY, Kim HM, Sun YK. Controlling the Wettability between Freestanding Electrode and Electrolyte for High Energy Density Lithium-Sulfur Batteries. *J Electrochem Soc*. 2018;165(1):A5006–13.
12. He J, Bhargava A, Manthiram A. Molybdenum Boride as an Efficient Catalyst for

- Polysulfide Redox to Enable High-Energy-Density Lithium–Sulfur Batteries. *Advanced Materials*. 2020 Oct 1;32(40).
13. Yang XX, Li XT, Zhao CF, Fu ZH, Zhang QS, Hu C. Promoted Deposition of Three-Dimensional Li₂S on Catalytic Co Phthalocyanine Nanorods for Stable High-Loading Lithium-Sulfur Batteries. *ACS Appl Mater Interfaces*. 2020 Jul 22;12(29):32752–63.
 14. Xu G, Yu D, Zheng D, Wang S, Xue W, Cao XE, et al. Fast Heat Transport Inside Lithium-Sulfur Batteries Promotes Their Safety and Electrochemical Performance. *iScience*. 2020 Oct 23;23(10).
 15. Hou LP, Zhang XQ, Yao N, Chen X, Li BQ, Shi P, et al. An encapsulating lithium-polysulfide electrolyte for practical lithium–sulfur batteries. *Chem*. 2022 Apr 14;8(4):1083–98.
 16. Wang R, Tang W, Tang M, Wu Q, Li J. ZIF-Derived Carbon Nanoframes as a Polysulfide Anchor and Conversion Mediator for High-Performance Lithium-Sulfur Cells. *ACS Appl Mater Interfaces*. 2021 May 12;13(18):21544–55.
 17. Wang X, Zhao C, Liu B, Zhao S, Zhang Y, Qian L, et al. Creating Edge Sites within the 2D Metal-Organic Framework Boosts Redox Kinetics in Lithium–Sulfur Batteries. *Adv Energy Mater*. 2022 Nov 10;12(42).
 18. Sun B, Wang D, Jiang Y, Wang R, Lyu L, Diao G, et al. Cyclodextrin Metal–Organic Framework Functionalized Carbon Materials with Optimized Interface Electronics and Selective Supramolecular Channels for High-Performance Lithium–Sulfur Batteries. *Advanced Materials*. 2024 Dec 27;
 19. Zeng Q, Xu L, Li G, Zhang Q, Guo S, Lu H, et al. Integrating Sub-Nano Catalysts into Metal-Organic Framework toward Pore-Confined Polysulfides Conversion in Lithium-Sulfur Batteries. *Adv Funct Mater*. 2023 Oct 18;33(43).
 20. Li Z, Wu J, Chen P, Zeng Q, Wen X, Wen W, et al. A new metallic composite cathode originated from hyperbranched polymer coated MOF for High-performance Lithium-Sulfur batteries. *Chemical Engineering Journal*. 2022 May 1;435.
 21. Xiao Y, Guo S, Xiang Y, Li D, Zheng C, Ouyang Y, et al. Engineering Configuration Compatibility and Electronic Structure in Axially Assembled Metal-Organic Framework Nanowires for High-Performance Lithium Sulfur Batteries. *ACS Energy Lett*. 2023 Dec 8;8(12):5107–15.
 22. Jiang J, Wu M, Li J, Zhou T, Xu B, Shan Z, et al. Three-Dimensional Covalent Organic Framework Serving as Host and Electrocatalyst in the Cathode of Li-S Battery. *Chemistry of Materials*. 2024 Nov 12;
 23. Du B, Luo Y, Yang Y, Xue W, Liu G, Li J. COFs-confined multifunctional Sulfur-host design towards High-performance Lithium-sulfur batteries. *Chemical Engineering*

- Journal. 2022 Aug 15;442.
24. Lin T, Wang H, Du X, Zhang D, Zhang Z, Liu G. A COF-coated MOF framework polysulfide barrier design for enhanced performance in lithium-sulfur batteries. *Electrochim Acta*. 2022 Apr 20;412.